Accepted Manuscript

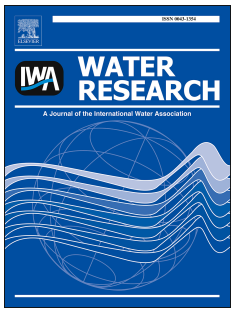

Phototransformation of halophenolic disinfection byproducts in receiving seawater: Kinetics, products, and toxicity

Jiaqi Liu, Xiangru Zhang, Yu Li, Wanxin Li, Chen Hang, Virender K. Sharma

PII: S0043-1354(18)30988-6

DOI: https://doi.org/10.1016/j.watres.2018.11.059

Reference: WR 14266

To appear in: *Water Research*

Received Date: 25 August 2018

Revised Date: 19 November 2018

Accepted Date: 21 November 2018

Please cite this article as: Liu, J., Zhang, X., Li, Y., Li, W., Hang, C., Sharma, V.K., Phototransformation of halophenolic disinfection byproducts in receiving seawater: Kinetics, products, and toxicity, *Water Research*, https://doi.org/10.1016/j.watres.2018.11.059.

Graphical Abstract

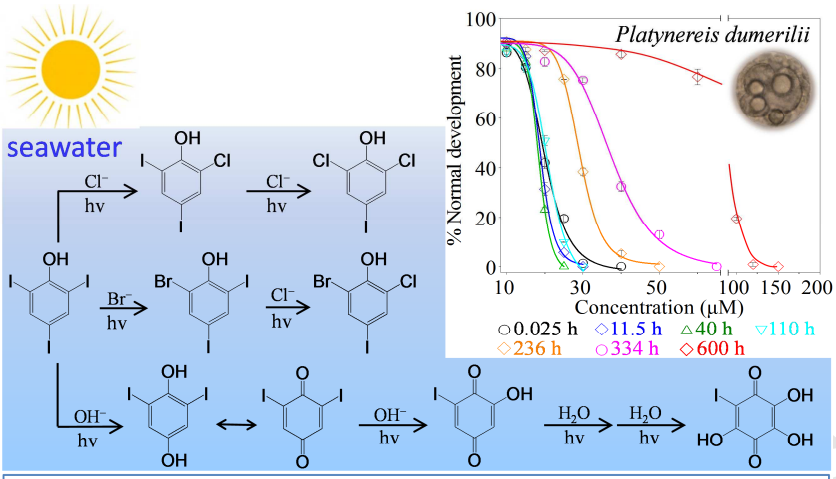

QSAR for phototransformation rate constant (k):

$$\log k = -0.0100 \times \Delta G_f^0 + 5.7528 \times \log MW + 0.3686 \times pKa - 19.1607$$

Phototransformation of halophenolic disinfection byproducts in receiving seawater: Kinetics, products, and toxicity

Jiaqi Liu[a,b], Xiangru Zhang[a,*], Yu Li[a], Wanxin Li[a], Chen Hang[a], Virender K. Sharma[b]

[a]*Department of Civil and Environmental Engineering, Hong Kong University of Science and Technology, Hong Kong SAR, China*

[b]*Department of Environmental and Occupational Health, School of Public Health, Texas A&M University, College Station, TX, USA*

[*] Corresponding author.
E-mail address: xiangru@ust.hk.

ABSTRACT

Flushing toilet with seawater is an effective method for preserving freshwater resources, but it introduces iodide and bromide ions into domestic wastewater. During chlorine disinfection, iodide and bromide ions in the saline wastewater effluent lead to the formation of iodinated and brominated aromatic disinfection byproducts (DBPs). Examples of aromatic DBPs include iodophenolic, bromophenolic and chlorophenolic compounds, which generally display substantially higher toxicity than haloaliphatic DBPs. This paper presented for the first time the rates of phototransformation of 21 newly identified halophenolic DBPs in seawater, the receiving waterbody of the wastewater effluent. The phototransformation rate constants (*k*) were in the range from 7.75×10^{-4} to 4.62×10^{-1} h^{-1}, which gave half-lives of 1.5 to 895 h. A quantitative structure−activity relationship was established for the phototransformation of halophenolic DBPs as $\log k = -0.0100 \times \Delta G_f^0 + 5.7528 \times \log MW + 0.3686 \times pKa - 19.1607$, where ΔG_f^0 is standard Gibbs formation energy, MW is molecular weight, and pK_a is dissociation constant. This model well predicted the *k* values of halophenolic DBPs. Among the tested DBPs, 2,4,6-triiodophenol and 2,6-diiodo-4-nitrophenol were found to exhibit relatively high risks on marine organisms, based on toxicity indices and half-lives. In seawater, the two DBPs underwent photonucleophilic substitutions by bromide, chloride and hydroxide ions, resulting in the conversion to their bromophenolic and chlorophenolic counterparts (which are less toxic than the parent iodophenolic DBPs) and to their hydroxyphenolic counterparts (iodo(hydro)quinones, which are more toxic than the parent iodophenolic DBPs). The formed iodo(hydro)quinones further transformed to hydroxyl-iodo(hydro)quinones, which have lower toxicity than precursor compounds.

Keywords: Disinfection byproducts, DBPs, photoconversion, phototransformation, toxicity.

1. Introduction

Flushing toilet with seawater is an effective method to conserve freshwater. This has been practiced in Hong Kong, Marshall Islands, Avalon, and Kiribati (Boehm et al., 2009; Yang et al., 2015; Liu et al., 2017). Consequently, the domestic wastewaters contain relatively high concentrations of inorganic ions such as iodide and bromide. In Hong Kong, the iodide and bromide ions in wastewater effluents have been found in the ranges of 30–60 µg/L and 20–31 mg/L, respectively (Gong and Zhang, 2013; Yang et al., 2015; Liu et al., 2017; Li et al., 2018; Gong et al., 2018). Chlorination of water, rich in bromide and iodide ions, generates a suite of brominated, iodinated, and chlorinated disinfection byproducts (DBPs) (Richardson et al., 2007; Agus et al., 2009; Song et al., 2010; Criquet et al., 2012; Tang et al., 2012; Roccaro et al., 2013; Bond et al., 2014; Hua et al., 2015; Zhu and Zhang, 2016; Sharma et al., 2017; Li and Mitch, 2018; Richardson and Postigo, 2018; Yan et al., 2016, 2018; Zhang et al., 2018; Gao et al., 2018; Jiang et al., 2018). There has been a growing concern regarding brominated and iodinated DBPs due to their substantially higher toxicity than that induced by the chlorinated counterparts (Echigo et al., 2004; Richardson et al., 2007; Dad et al., 2013; Yang and Zhang, 2013; Liu and Zhang, 2014; Sharma et al., 2014). In recent years, different groups of halophenolic DBPs have been identified in chlorinated wastewater effluents, including 5-halosalicylic acids, 4-halophenols, 2,4-dihalophenols, 2,6-dihalophenols, 2,4,6-trihalophenols, 2,6-dihalo-4-nitrophenols, 3,5-dihalo-4-hydroxybenzaldehydes, 3,5-dihalo-4-hydroxybenzoic acids, and 2,5-dibromohydroquinone (Yang and Zhang, 2016). Toxicity of twenty halophenolic DBPs and five haloaliphatic DBPs has been evaluated by measuring the growth inhibition to the marine alga *Tetraselmis marina* and the developmental toxicity to the marine polychaete *Platynereis dumerilii* (Liu and Zhang, 2014; Yang and Zhang, 2013). The results revealed that halophenolic

DBPs generally induced dozens to hundreds of times higher toxicity than haloaliphatic DBPs. Moreover, of the halophenolic DBPs tested, 2,4,6-triiodophenol exhibited the highest growth inhibition to the marine alga; 2,6-diiodo-4-nitrophenol and 2,4,6-triiodophenol were two of the most toxic DBPs to the marine polychaete (Liu and Zhang, 2014; Yang and Zhang, 2013).

Chlorinated saline wastewater effluents containing DBPs are continuously discharged into seawater (the ultimate receiving water body), and consequently halophenolic DBPs (especially iodophenolic and bromophenolic ones) might chronically do harm to marine species (Yang et al., 2015). Fortunately, the solar irradiation could transform most of toxic DBPs to less toxic products, causing a decrease in the toxicity of wastewater effluents (mixtures of all DBPs) (Liu et al., 2017; Lv et al., 2017). However, some toxic halogenated DBPs were likely persistent in receiving seawater (Fig. S1 in the Supplementary Information). Although great progress has been made to understand phototransformation of DBPs from the mixture point of view, information on individual halophenolic DBPs is still lacking.

Recently, the quantitative structure–activity relationship (QSAR) approach has been increasingly applied in studies of emerging water contaminants to establish relationships between experimental (including chemical and toxicological) observations and physicochemical properties of the molecules (Yang and Zhang, 2013; Liu and Zhang, 2014; Xiao et al., 2015; Jin et al., 2015; Borhani et al., 2016; Wang et al., 2018). This approach enables prediction of properties on the assumption that compounds with similar structures behave alike and that the property differences are attributable to enthalpy changes caused by different types and numbers of functional groups (Chen, 2011). Different QSAR models have been developed for the hydrolysis of DBPs (Wang et al., 2018; Yu and Reckhow, 2015; Chen, 2011; Glezer et al., 1999). Currently, a large number of DBPs (especially the toxic halophenolic ones) in chlorinated

wastewater effluents are still unknown, and might be gradually identified and confirmed in future studies. It is important to develop a QSAR model for phototransformation of halopenolic DBPs, enabling prediction of the stability of halophenolic DBPs which were not included in this study.

Accordingly, the present paper aimed to: (i) investigate the phototransformation kinetics of various groups of halophenolic DBPs; (ii) develop a QSAR model for the phototransformation kinetics of halophenolic DBPs; (iii) delineate the phototransformation mechanisms of two selected iodophenolic DBPs, 2,4,6-triiodophenol and 2,6-diiodo-4-nitrophenol (which are of relatively high risks to marine organisms as shown later in the Results and Discussion) in seawater by identifying products and transformation pathways; and (iv) evaluate toxicity variations of the two iodophenolic DBPs during transformation against the marine polychaete *P. dumerilii*. This species has been successfully used in measuring the comparative toxicity of various DBPs, wastewater effluent and drinking water samples (Yang and Zhang, 2013; Yang et al., 2015; Liu et al., 2015; Liu et al., 2017; Li et al., 2017; Jiang et al., 2017; Han et al., 2017; Han and Zhang, 2018).

2. Materials and methods

2.1. Chemicals, solvents and experimental setup

Ultrapure water (18.2 MΩ·cm) was supplied by a NANOpure system (Barnstead). Seawater was collected from Clear Water Bay, Hong Kong (22.3 ºN, 114.2 ºE). The pH of seawater was 8.2 and concentrations of iodide, bromide, chloride, nitrate, and total organic carbon (TOC) were 32.1 μg/L, 64 mg/L, 19200 mg/L, <0.025 mg/L as N, and 1.1 mg/L as C, respectively. The iodide concentration was quantified per the method by Gong and Zhang (2013). Bromide, chloride and nitrate were measured with an ion chromatograph (Dionex). TOC was measured

with a TOC analyzer (Shimadzu). Prior to use, the seawater was filtered with a 0.45 μm filter, autoclaved at 121 ºC for 20 min, and cooled to ambient temperature. Additionally, the seawater was further aerated for 15 min for cultivating the polychaete. Standard compounds of DBPs were purchased from different suppliers, with details shown in Table S1. Other chemicals and organic solvents were purchased from Sigma–Aldrich.

In phototransformation studies, 100-mL quartz flasks (base diameter 67 mm, overall height 110 mm, neck diameter 22 mm, neck length 25 mm) were obtained from Technical Glass Products Inc., U.S. Eight full-spectrum simulated sunlight lamps (BlueMax Spectra 5900 47" T5 High Definition Fluorescent Tube) were acquired from Full Spectrum Solutions, U.S., and the spectrum is shown in Fig. S2. A chamber with length × width × height of 1180 mm × 485 mm × 615 mm was self-constructed in the lab. The simulated sunlight lamps were fixed at the top of the chamber and the distance between two adjacent lamps was 60 mm. The light intensity at the bottom of the chamber was calculated as 6134 ± 231 lux (equivalent to 48.5 ± 1.8 W/m^2, per details shown in Fig. S3). The temperature in the chamber was controlled at 22 ºC. This chamber could hold totally 96 100-mL quartz flasks. During each test, the 96 quartz flasks each containing a 40 mL solution (i.e., a certain number of flasks contained DBP test solutions, depending on the experimental design, and the other flasks contained seawater) were placed in the chamber. The quartz flasks were repositioned each 2 h to eliminate the difference in locational illumination. The volume of each test solution was daily measured and replenished to 40 mL by adding ultrapure water to compensate for evaporation loss.

2.2. Phototransformation of 21 halophenolic DBPs in seawater

The phototransformation of 21 halophenolic DBPs (as shown in Table 1) in seawater was studied. These DBPs were newly identified in chlorinated saline wastewater effluents (Yang et

al., 2013; Ding et al., 2013). For each DBP, ~20 mg standard compound was dissolved in 4 L seawater to obtain a solution at 5 mg/L, and the solution was quickly adjusted to pH 8.2 (i.e., the pH of seawater) with NaOH and HCl solutions. Then, four 40 mL solutions were taken out and placed into 100 mL quartz flasks. Two aliquots (as duplicates) were exposed to simulated sunlight for 84 h, and then pretreated, followed by the analysis with a Waters Acquity ultra performance liquid chromatograph/electrospray ionization-triple quadrupole mass spectrometer (UPLC/ESI-tqMS). Details are shown in the Supplementary Information. The other two duplicate aliquots were pretreated and analyzed immediately after preparation.

2.3. QSAR modelling

In QSAR modeling, the logarithm of the reaction rate constant (log *k*) was used as the dependent (Wang et al., 2018). Physiochemical parameters were selected as independent variables (molecular descriptors) based on the phototransformation mechanism of halophenolic DBPs. Multiple regression analyses were performed with the software STATISTICA 12.0 (StatSoft). The quality of the model was characterized by the square of correlation coefficient (r^2), the Fisher criterion (F), the significance level (p), and the standard error of estimate (σ).

2.4. Phototransformation and toxicity variation of 2,4,6-triiodophenol and 2,6-diiodo-4-nitrophenol in seawater

A 3 L solution of 2,4,6-triiodophenol (or 2,6-diiodo-4-nitrophenol) was prepared by dissolving the standard compound in seawater at 5 mg/L. The pH of seawater remained the same after the addition of 2,4,6-triiodophenol (or 2,6-diiodo-4-nitrophenol) at this low concentration. Then the solution was divided into 72 portions, and each portion was 40 mL and placed into a

100 mL quartz flask.

Seventy portions were divided evenly into seven groups and put under the irradiation of simulated sunlight for seven exposure times (0.025–600 h for 2,4,6-triiodophenol and 0.025–684 h for 2,6-diiodo-4-nitrophenol). After a specific exposure time, two duplicate portions were pretreated following the same procedure as that for the solutions of the 21 DBPs as shown in Supplementary Information. Then, the duplicate pretreated solutions were combined into one solution, and subjected to precursor ion scan (PIS), product ion scan, and multiple reaction monitoring (MRM) analyses using UPLC/ESI-tqMS. PIS of *m/z* 126.9 is a powerful method for fast, selectively, and sensitively detecting iodine-containing compounds (Gong and Zhang, 2015). For identifying and monitoring iodine-containing phototransformation products, UPLC/ESI-tqMS MRM scan and product ion scan were performed. The structure of each product was proposed according to the retention time, the isotopic ratio of the ion cluster, and the fragment information in product ion scans. The other eight portions of 2,4,6-triiodophenol (or 2,6-diiodo-4-nitrophenol) seawater solutions in each group were combined into a 320 mL solution. After specific pretreatment, duplicate developmental toxicity tests were conducted with the embryos of a marine polychaete *P. dumerilii* following the procedure in previous studies (Yang et al., 2015; Liu et al., 2017) (see details in the Supplementary Information).

The remaining two portions were kept in darkness for 600 h for 2,4,6-triiodophenol (or 684 h for 2,6-diiodo-4-nitrophenol). These samples were pretreated and analyzed with UPLC/ESI-tqMS following the same procedure as that for the solutions exposed to light.

3. Results and discussion

3.1. Phototransformation rates of 21 halophenolic DBPs

The phototransformation of 21 halophenolic DBPs in seawater within 84 h of light exposure was investigated. The degradation of these DBPs followed pseudo-first-order reactions, according to our previous study (Liu et al., 2017). Table 1 lists the percentages of the phototransformation of DBPs within 84 h light exposure. The calculated pseudo-first-order rate constants (k, h^{-1}) and half-lives (h) are also given in Table 1. The results suggested that iodophenolic DBPs were transformed faster than their bromophenolic counterparts, which in turn were transformed faster than their chlorophenolic counterparts. For the four groups of DBPs tested (2,4,6-trihalophenols, 4-halophenols, 2,6-dihalo-4-nitrophenols, and 3,5-dihalo-4-hydroxybenzaldehydes), the descending order of the phototransformation rates within each group was: 2,4,6-triiodophenol > 2,4,6-tribromophenol > 2,4,6-trichlorophenol; 4-iodophenol > 4-bromophenol > 4-chlorophenol; 2,6-diiodo-4-nitrophenol > 2,6-dibromo-4-nitrophenol > 2,6-dichloro-4-nitrophenol; 3,5-diiodo-4-hydroxybenzaldehyde > 3,5-dibromo-4-hydroxybenzaldehyde > 3,5-dichloro-4-hydroxybenzaldehyde. Abusallout and Hua (2016a) and Wang et al. (2017) studied the photolysis of haloaliphatic DBP analogues and also observed the same descending order of photolysis rates: iodinated DBPs > brominated counterparts > chlorinated counterparts.

To better understand and capture the roles of functional groups on the photolytic stability of halophenolic DBPs, the k values were interpreted using a QSAR model. The standard Gibbs energies of formation (ΔG_f^0) of DBPs may represent their relative stability. The ΔG_f^0 value of each DBP was calculated using the software Chem3D Ultra 8.0 (CambridgeSoft) and given in Table S2. A regression analysis of log k versus ΔG_f^0 was conducted (Equation (1) and Table S3).

$$\log k = -0.00319 \times \Delta G_f^0 - 2.58277 \qquad (1)$$

$r^2 = 0.3098$, $F(1,19) = 8.5282$, $p = 0.00877$, $\sigma = 0.5778$.

The low correlation coefficient suggests that other factors also contribute to the *k* values of halophenolic DBPs. The authors' previous research demonstrated that halophenolic DBPs underwent S_N2 photonucleophilic substitution when they entered receiving seawater: bromophenolic and iodophenolic DBPs were converted to their chlorophenolic or hydroxyphenolic counterparts, via substituting the bromine and iodine atoms with chloride or hydroxide ions in seawater; chlorophenolic DBPs were converted to their hydroxyphenolic counterparts, via substituting the chlorine atoms with hydroxide ions in seawater (Liu et al., 2017). As shown later in this manuscript, besides chloride and hydroxide ions, iodophenolic DBPs were also substituted by bromide ions to form their brominated counterparts. Accordingly, we considered the substitution possibilities (P_{sub}) as one factor affecting the phototransformation rate constant. P_{sub} is related to the number of each type of halogen atoms in a halophenol (*n*) and the number of substitution types of one halogen type (*m*), and we defined it as the sum of the products of *n* and *m* of all halogen types, i.e., $\sum(n \times m)$. For iodine, *m* is 3 as it can be substituted by Br^-, Cl^- and OH^-; for bromine, *m* is 2 as it can be substituted by Cl^- and OH^-; for chlorine, *m* is 1 as it can be substituted by OH^- only. The calculation of the P_{sub} value of 2-bromo-4-chlorophenol is exemplified here. This halophenol contains one chlorine atom and one bromine atom, so its P_{sub} can be calculated as 1×1 + 1×2 = 3. The P_{sub} values of the tested DBPs are presented in Table S2. A multiple regression analysis of log *k* versus ΔG_f^0 and log P_{sub} was conducted, and a QSAR was obtained (Equation (2) and Table S3).

$$\log k = -0.00528 \times \Delta G_f^0 + 1.69789 \times \log P_{sub} - 3.58772 \qquad (2)$$

$r^2 = 0.5584$, $F(2,18) = 11.381$, $p = 0.00064$, $\sigma = 0.4749$.

To further improve the prediction of the *k* values, ionization of halophenolic DBPs in seawater was considered. In the S_N2 photonucleophilic substitution of each halophenolic DBP,

the nucleophile (bromide, chloride, or hydroxide) attacks on the DBP to form an unstable complex (Liu et al., 2017). Compared with the neutral form, the negatively charged form of a halophenolic DBP might be difficult to be attacked because of the charge repulsion. Logarithmic dissociation constant (pK_a) is a quantitative measure of ionization of a halophenolic DBP in seawater. The pK_a values of the tested DBPs at 25 °C, obtained from SciFinder, are given in Table S2. By including pK_a as a descriptor, the QSAR was significantly improved, as shown in Equation (3) and Table S3. A plot of measured log *k* versus predicted log *k* is shown in Fig. 1a.

$$\log k = -0.01028 \times \Delta G_f^0 + 3.21592 \times \log P_{sub} + 0.27402 \times pK_a - 6.50578 \quad (3)$$

$r^2 = 0.8365$, $F(3,17) = 28.987$, $p < 0.00000$, $\sigma = 0.2973$.

Wang et al. (2018) analyzed the hydrolysis rates of aliphatic DBPs, and found that iodinated DBPs hydrolyzed faster than their brominated counterparts, which in turn hydrolyzed faster than their chlorinated counterparts. They established a QSAR model for the hydrolysis of aliphatic DBPs, using molecular weight (MW) (because the atomic weight of halogen follows the rank order of iodine > bromine > chlorine) and the total number of halogen atoms in a DBP molecule as descriptors. Accordingly, the QSAR model of Equation (3) was modified by replacing log P_{sub} with log MW and adding the logarithm of the total number of halogen atoms in a molecule (log *N*) as a descriptor, as shown in Equation (4) and Table S3.

$$\log k = -0.0107 \times \Delta G_f^0 + 5.5409 \times \log MW + 0.3920 \times pKa + 0.9085 \times \log N - 19.1031 \quad (4)$$

$r^2 = 0.8752$, $F(4,16) = 28.041$, $p < 0.00000$, $\sigma = 0.2678$.

The model was slightly improved, but log *N* is "insignificant" in this regression ($p > 0.05$, Table S3). This indicates that the multiple regression should be re-conducted by removing log *N*. As shown in Equation (5), r^2 of the regression slightly decreased because the removal of one descriptor, but the F value significantly increased. The plot of measured log *k* versus predicted

log k using Equation (5) is shown in Fig. 1b.

$$\log k = -0.0100 \times \Delta G_f^0 + 5.7528 \times \log MW + 0.3686 \times pKa - 19.1607 \quad (5)$$

$r^2 = 0.8474$, $F(3,17) = 31.469$, $p < 0.00000$, $\sigma = 0.2872$.

The insignificant contribution of log N to the QSAR model might result from the positive correlation between MW and N. For a group of halophenolic DBP analogues, the MW increase with the increase of the total number of halogen atoms on the benzene ring, e.g., the MWs of chlorophenols follow the rank order of chlorophenol (128.6) < dichlorophenol (163.0) < trichlorophenol (197.5). Equations (3) and (5) are both statistically acceptable, and Equation (5) is slightly better. Besides, the concept and calculation of P_{sub} are somewhat complicated, while the calculation of MW is easier. Accordingly, Equation (5) is adopted as the QSAR model for the phototransformation of halophenolic DBPs.

It should be pointed out that the phototransformation of halophenolic DBPs in natural marine environment mainly depends on the actual intensity of sunlight and the penetration of sunlight in seawater. The solar intensity on horizontal surface depends on the solar elevation angle. Tables S4–S6 show the solar elevations and intensities on horizontal surface in three coastal regions with different latitudes, including Singapore (1.3° N 103.8° E), Hong Kong (22.3° N 114.2° E), and Boston, MA, U.S. (42.4° N 71.0° W), on March 20, 2018 (when the sun directed at the equator). In this study, halophenolic DBP solutions were contained in 100 mL quartz flasks, with the water depth of ~1.1 cm, and the sunlight (6134 ± 231 lux) penetration could be considered as 100%. In natural marine water, the penetration of sunlight decreased with water depth (Liu et al., 2017). The phototransformation rates of halophenolic DBPs might vary with actual sunlight intensity received by the DBPs in seawater. The kinetics data and QSAR model obtained in this study show the “comparative” k values of halophenolic DBPs, which may

aid in determining the persistent DBPs.

The authors' group previously evaluated the toxicity of the 21 tested halophenolic DBPs using a marine alga and a marine polychaete (Liu and Zhang, 2014; Yang and Zhang, 2013). The EC_{50} value of each DBP against each marine species is listed in Table S7. The toxicity index was calculated as the reciprocal of the EC_{50} value × 1000 (Pan et al., 2014). The risk of each halophenolic DBP on the alga or the polychaete was calculated as the product of the toxicity index and the half-life (Table S7). 2,4,6-Triiodophenol and 2,6-diiodo-4-nitrophenol showed relatively high risks among the 21 halophenolic DBPs, suggesting that these two DBPs deserve more attention. Thus, the phototransformation of 2,4,6-triiodophenol and 2,6-diiodo-4-nitrophenol was further investigated.

3.2. Phototransformation and toxicity variation of 2,4,6-triiodophenol in seawater

When the 2,4,6-triiodophenol solutions were kept in darkness for 600 h, no change in concentration was observed, indicating that no transformation of 2,4,6-triiodophenol occurred without light irradiation. Fig. 2 shows the ESI-tqMS PIS spectra of *m/z* 126.9 of 2,4,6-triiodophenol solutions at different light exposure times. The intensity of ion *m/z* 471 (corresponding to 2,4,6-triiodophenol) decreased with light exposure time, indicating the phototransformation of 2,4,6-triiodophenol. Several phototransformation products were detected (Table S8). After 0.025 h light exposure, diiodohydroquinone (*m/z* 361, including 2,6-diiodo-1,4-hydroquinone and 2,4-diiodo-1,6-hydroquinone) was detected in the solution, and it might be generated via the substitution of an iodine atom in 2,4,6-triiodophenol with a hydroxyl group. Additionally, diiodohydroquinone was in equilibrium with diiodoquinone (*m/z* 360, including 2,6-diiodo-1,4-quinone and 2,4-diiodo-1,6-quinone). UPLC/ESI-tqMS MRM scans of ions *m/z* 361 and *m/z* 360 were conducted for all solutions. The variation in the total peak area (i.e., the

summation of the peak areas of ions *m/z* 361 and *m/z* 360) with exposure time indicates the change in the concentration of diiodohydroquinone. As shown in Fig. S4, diiodohydroquinone formed and subsequently converted, with the maximum concentration showing up at the light exposure time of 40 h. After 11.5 h of light exposure, chlorodiiodophenol (*m/z* 379/381) and bromodiiodophenol (*m/z* 423/425) were detected (Fig. 2), and they might form from the halogen atom substitution in 2,4,6-triiodophenol (i.e., via the substitution of iodine atom by chloride and bromide, respectively).

The substitution of iodine by hydroxide, chloride and bromide ions may follow the S_N2 photonucleophilic substitution mechanism (Liu et al., 2017) as follows:

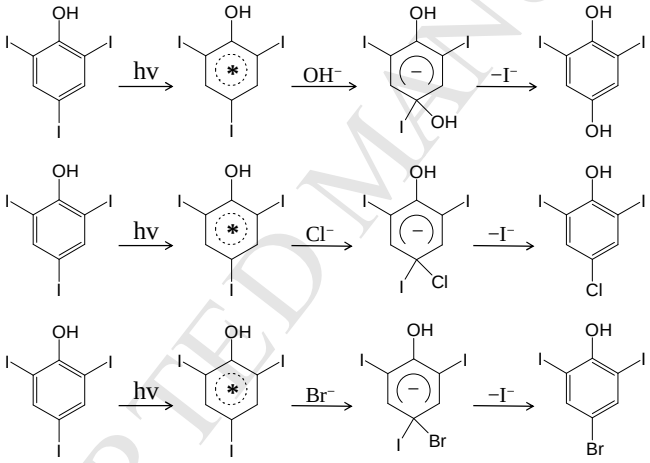

When exposed to the simulated sunlight, 2,4,6-triiodophenol became excited. The iodine atoms are at the para- and ortho-positions to the hydroxyl group (an electron donating group), and thus are readily substituted. In seawater, hydroxide, chloride and bromide ions could serve as nucleophiles. They added to the photo-excited 2,4,6-triiodophenol molecules to generate unstable δ-complexes, e.g., 4,4-hydroxyiodo-2,6-diiodophenol, 4,4-chloroiodo-2,6-diiodophenol, and 4,4-bromoiodo-2,6-diiodophenol, respectively. These δ-complexes tended to transform to stable compounds by leaving either one functional group on the 4-position. Because the dissociation energies follow the rank order of C_6H_5–I (272.0 kJ/mol) < C_6H_5–Br (336.4 kJ/mol) < C_6H_5–Cl

(399.6 kJ/mol) < C_6H_5–OH (463.6 kJ/mol) (Cottrell, 1958), the iodine atom left as an I^- ion in all the three δ-complexes, yielding the substitution products 2,6-diiodo-1,4-hydroquinone, 4-chloro-2,6-diiodophenol and 4-bromo-2,6-diiodophenol.

In the UPLC/ESI-tqMS MRM chromatograms of ion clusters *m/z* 379/381 and *m/z* 423/425 (Fig. S5 and S6), two peaks were observed for each ion cluster. Accordingly, ion cluster *m/z* 379/381 might correspond to 4-chloro-2,6-diiodophenol and 2-chloro-4,6-diiodophenol, and ion cluster *m/z* 423/425 might correspond to 4-bromo-2,6-diiodophenol and 2-bromo-4,6-diiodophenol. This suggested that the iodine atoms at both para- and ortho-positions to the hydroxyl group might be substituted. The peak areas of chlorodiiodophenol and bromodiiodophenol (as the summation of both isomers) increased from the exposure time of 11.5 to 110 h and then decreased (Fig. S4–S6). The decrease resulted from further photonucleophilic substitution.

After 110 h light exposure, dichloroiodophenol (*m/z* 287/289/291) and bromochloroiodophenol (*m/z* 331/333/335) were detected (Fig. 2), and they were the products of photonucleophilic chlorine substitution of chlorodiiodophenol and bromodiiodophenol, respectively. According to the UPLC/ESI-tqMS MRM chromatograms (Figs. S7 and S8), two dichloroiodophenols (2,6-dichloro-4-iodophenol and 2,4-dichloro-6-iodophenol) and one bromochloroiodophenol (2-bromo-6-chloro-4-iodophenol) were generated. The peak areas of dichloroiodophenol (as the summation of both isomers) and 2-bromo-6-chloro-4-iodophenol increased from the exposure time of 110 to 334 h and then decreased (Figs. S4, S7, and S8). Accordingly, photonucleophilic substitution played an important role in the transformation of 2,4,6-triiodophenol in seawater (Fig. 3a). Photonucleophilic hydroxyl substitution was observed in the photodegradation of 2-chlorophenol (Rao et al., 2003), and photonucleophilic chlorine

343 substitution was found in phototransformation of iodophenolic and bromophenolic DBPs in
344 seawater (Liu et al., 2017). This is the first time that the photonucleophilic bromine substitution
345 of iodophenolic DBPs was observed.

346 After 236 h light exposure, iodotrihydroxyquinone (*m/z* 282) was observed (Fig. 2), and its
347 peak area in UPLC/ESI-tqMS MRM chromatogram kept increasing within the exposure period
348 from 236 to 600 h (Fig. S4). Iodotrihydroxyquinone was proposed to be a transformation product
349 of diiodoquinone, as exemplified by the transformation of 2,6-diiodo-1,4-quinone (Fig. 3b).
350 First, 2,6-diiodo-1,4-quinone underwent two sequential photo-addition reactions with water,
351 leading to two more hydroxyl groups substituted on the benzene ring and the formation of 2,6-
352 diiodo-3,5-dihydroxy-1,4-quinone (with the mechanism shown in Fig. S9a–b). Second, 2,6-
353 diiodo-3,5-dihydroxy-1,4-quinone was transformed to 2-iodo-3,5,6-trihydroxy-1,4-quinone via
354 photonucleophilic hydroxyl substitution. Another possible pathway is that 2,6-diiodo-1,4-
355 quinone was first transformed to 2-hydroxy-6-iodo-1,4-quinone via photonucleophilic hydroxyl
356 substitution, and then 2-hydroxy-6-iodo-1,4-quinone underwent two sequential photo-addition
357 reactions with water, generating 2-iodo-3,5,6-trihydroxy-1,4-quinone (with the mechanism
358 shown in Fig. S9c–d). The mechanism of photo-addition reaction between haloquinone and
359 water under UV radiation has been suggested earlier (Qian et al., 2013).

360 Fig. 4a shows the normal development percentages of the marine polychaete embryos in the
361 2,4,6-triiodophenol solutions with different light exposure times. Notably, each concentration in
362 Fig. 4a was the concentration of 2,4,6-triiodophenol in the concentrated sample before
363 phototransformation. For each curve, the value of EC_{50} was calculated per Yang and Zhang
364 (2013)'s method. According to the previous study (Yang and Zhang, 2013), the EC_{50} values of
365 the same DBP solution from three different batches of embryos were within a relative standard

366 deviation of 1.2%.

367 Photonucleophilic bromine and chlorine substitution triggered the transformation from
368 2,4,6-triiodophenol to its bromophenolic and chlorophenolic counterparts, which might decrease
369 the toxicity of "2,4,6-triiodophenol" (to be exact, the overall toxicity of "2,4,6-triiodophenol and
370 its transformation products"). However, per the EC_{50} values (Table S9), when the exposure time
371 increased from 0.025 to 40 h, the toxicity of "2,4,6-triiodophenol" slightly increased (by 7.6%).
372 This toxicity increase agrees with the concentration increase of diiodo(hydro)quinone.
373 Halo(hydro)quinones are a new class of highly toxic DBPs in disinfected wastewater and
374 drinking water. Halohydroquinones were found to be substantially more toxic than other
375 halophenolic DBPs (Yang and Zhang, 2013). Certain haloquinones generated intracellular
376 reactive oxygen species in T24 bladder cancer cells, and bound to oligodeoxynucleotides
377 (Anichina et al., 2010; Du et al., 2013). When the light exposure time exceeded 40 h, the
378 concentration of diiodo(hydro)quinone decreased, and the toxicity of "2,4,6-triiodophenol" also
379 decreased. This indicates that further phototransformation of diiodo(hydro)quinone was a
380 detoxification process. Photo-addition reaction with water led to more substitutions of hydroxyl
381 groups on the benzene ring, which lowered log K_{ow} of the (hydro)quinone product and thus
382 lowered the toxicity of the product. This is consistent with the results of the previous study (Liu
383 et al., 2017). After 600 h of light exposure, the toxicity of "2,4,6-triiodophenol" decreased by
384 78%, compared with the initial toxicity.

385

386 ***3.3. Phototransformation and toxicity variation of 2,6-diiodo-4-nitrophenol in seawater***

387 The concentration of 2,6-diiodo-4-nitrophenol in the solution kept under darkness for 684 h
388 was almost the same as the initial concentration, suggesting that no transformation occurred. Fig.

S10 shows the ESI-tqMS PIS spectra of *m/z* 126.9 of 2,6-diiodo-4-nitrophenol seawater solutions with different light exposure times. The intensity of ion *m/z* 390 (corresponding to 2,6-diiodo-4-nitrophenol) decreased with the light exposure time, suggesting the occurrence of phototransformation. After 11.5 h light exposure, 2-chloro-6-iodo-4-nitrophenol (*m/z* 298/300) and 2-bromo-6-iodo-4-nitrophenol (*m/z* 342/344) were formed via the photonucleophilic chlorine and bromine substitutions of 2,6-diiodo-4-nitrophenol, respectively. The ion intensity of 2-chloro-6-iodo-4-nitrophenol increased from the exposure time of 11.5 to 110 h and stayed the same afterwards, and the ion intensity of 2-bromo-6-iodo-4-nitrophenol increased from the exposure time of 11.5 to 110 h and decreased afterwards. Interestingly, 2,6-diiodo-1,4-hydroquinone (*m/z* 361) was generated via the substitution of the nitro group in 2,6-diiodo-4-nitrophenol with a hydroxyl group. This photonucleophilic substitution occurred because the C_6H_5–OH bond (463.6 kJ/mol) shows higher dissociation energy than the C_6H_5–NO_2 bond (215.5 kJ/mol) (Cottrell, 1958), and also because the nitro group is at the meta-position of both iodine atoms (electron withdrawing groups) and the para-position of the hydroxyl group (an electron donating group) (Liu et al., 2017). 2,6-Diiodo-1,4-hydroquinone was in equilibrium with 2,6-diiodo-1,4-quinone (*m/z* 360) in water. The total intensity of ions *m/z* 360 and *m/z* 361 increased from the exposure time of 11.5 to 40 h, then decreased afterwards, and became undetectable after 362 h of light exposure. Further transformation of 2,6-diiodo-1,4-(hydro)quinone should follow the reactions as observed in the phototransformation of 2,4,6-triiodophenol. At the exposure time of 110 h, another photonucleophilic hydroxyl substituted product, 2-iodo-4-nitro-1,6-hydroquinone (*m/z* 280), was detected. This compound was in equilibrium with 2-iodo-4-nitro-1,6-quinone (*m/z* 279). The total intensity of ions *m/z* 280 and *m/z* 279 increased from the exposure time of 110 to 684 h. Within 684 h of light exposure, the

main reactions for the transformation of 2,6-diiodo-4-nitrophenol were photonucleophilic bromine, chlorine and hydroxyl substitutions (Fig. S11). Interestingly, 33% of 2,6-diiodo-4-nitrophenol remained after 684 h of light exposure, while 2,4,6-triiodophenol was undetectable after 600 h of light exposure (Fig. 2). This confirmed that the phototransformation of 2,6-diiodo-4-nitrophenol (*m/z* 390) was slower than that of 2,4,6-triiodophenol.

Fig. 4b shows the normal development percentages of the marine polychaete embryos in the 2,6-diiodo-4-nitrophenol solutions with different light exposure times. Per the EC_{50} values (Table S10), the toxicity of "2,6-diiodo-4-nitrophenol" (to be exact, the overall toxicity of "2,6-diiodo-4-nitrophenol and its transformation products") increased by 14.9% within the first 40 h of light exposure, which matched well with the intensity increase of 2,6-diiodo-1,4-(hydro)quinone. This confirmed that the formation of halo(hydro)quinone increased the toxicity. With further phototransformation of 2,6-diiodo-1,4-(hydro)quinone from the exposure time of 40 to 110 h, the toxicity of "2,6-diiodo-4-nitrophenol" decreased. Later, another toxic haloquinone product, 2-iodo-4-nitro-1,6-(hydro)quinone was generated, and its ion intensity increased with the exposure time; as a result, the toxicity of "2,6-diiodo-4-nitrophenol" kept slightly increasing within the exposure period from 110 to 684 h. From these results, it can be concluded that 2,6-diiodo-4-nitrophenol is a relatively persistent DBP with relatively high toxicity in receiving seawater. Besides, 2,6-dibromo-4-nitrophenol and 2,6-dichloro-4-nitrophenol also showed low phototransformation rates (Table 1). It is expected that different (hydro)quinone products might also form during the phototransformation of these two DBPs, and their toxicity might maintain at relatively high levels after a long exposure time. Accordingly, controlling the formation of halonitrophenolic DBPs deserves a high priority in wastewater treatment.

It needs mentioning that, according to Abusallout and Hua (2016b), sunlight irradiation of

nitrate and natural organic matter (NOM) in water could result in the formation of HO·, NO· and NO_2· radicals and excited NOM triplet state that could cause the indirect phototransformation of halophenolic DBPs. On the other hand, sunlight irradiation could convert halide ions in seawater to halogen radicals (Yang and Pignatello, 2017) that could react with NOM in seawater to form halogenated organics (Sankoda et al., 2017; Calza et al., 2008). As assessed in Supplementary Information, compared with the phototransformation of halophenolic DBPs, either the indirect phototransformation of or the formation of halophenolic DBPs in the seawater under sunlight irradiation might be negligible.

4. Conclusions

This study investigated the phototransformation of 21 halophenolic DBPs in receiving seawater. The reaction rate constants (k, h^{-1}) were well predicted using a QSAR model that employed three physicochemical descriptors, ΔG_f^0, log MW and pK_a. Among the tested DBPs, 2,4,6-triiodophenol and 2,6-diiodo-4-nitrophenol exhibited relatively high risks (i.e., relatively high toxicity and long half-life) on marine organisms. These two iodophenolic DBPs were transformed to their bromophenolic, chlorophenolic, and hydroxyphenolic counterparts via photonucleophilic substitutions by bromide, chloride and hydroxide ions in seawater.

By combining with our previous study (Liu et al., 2017), it can be concluded that the toxicity of a halophenolic DBP changed during its phototransformation in receiving seawater. Photonucleophilic bromine and chlorine substitutions might decrease the toxicity of iodophenolic DBPs, and photonucleophilic chlorine substitution might decrease the toxicity of bromophenolic DBPs. However, via photonucleophilic hydroxyl substitution, halophenolic DBPs were transformed to their hydroxyphenolic analogues, halo(hydro)quinones, and the toxicity might

458 significantly increase. Fortunately, halo(hydro)quinones could further transform to less toxic
459 products. As expected, the variation in toxicity of a halophenolic DBP in receiving seawater
460 mainly depended on the formation and further transformation of its hydroxyphenolic counterpart,
461 halo(hydro)quinone.

462

463 **Acknowledgments**

464 This study was financially supported by the Research Grants Council of Hong Kong,
465 Theme-based Research Scheme (No. T21-711/16R) and Collaborative Research Fund (No.
466 C7044-14G). Jiaqi Liu was also supported by the U.S. National Institutes of Health institutional
467 training grant T32 ES026568. The authors thank Yulan Ouyang, Yan Hang Ho and Shueng Yu
468 Sin for preparing and pretreating samples.

469

470 **Appendix A. Supplementary data**

471 Supplementary data associated with this article can be found, in the online version, at
472 http://dx.doi.org.

473

474 **References**

475 Abusallout, I., Hua, G., 2016a. Photolytic dehalogenation of disinfection byproducts in water by
476 natural sunlight irradiation. Chemosphere 159, 184–192.
477 Abusallout, I., Hua, G., 2016b. Natural solar photolysis of total organic chlorine, bromine and
478 iodine in water. Water Res. 92, 69–77.
479 Agus, E., Voutchkov, N., Sedlak, D.L., 2009. Disinfection by-products and their potential impact
480 on the quality of water produced by desalination systems: A literature review. Desalination

237, 214–237.

Anichina, J., Zhao, Y., Hrudey, S.E., Le, X.C., Li, X.-F., 2010. Electrospray ionization mass spectrometry characterization of interactions of newly identified water disinfection byproducts halobenzoquinones with oligodeoxynucleotides. Environ. Sci. Technol. 44, 9557–9563.

Boehm, A.B., Yamahara, K.M., Love, D.C., Peterson, B.M., McNeill, K., Nelson, K.L., 2009. Covariation and photoinactivation of traditional and novel indicator organisms and human viruses at a wastewater-impacted marine beach. Environ. Sci. Technol. 43, 8046–8052.

Bond, T., Huang, J., Graham, N.J.D., Templeton, M.R., 2014. Examining the interrelationship between DOC, bromide and chlorine dose on DBP formation in drinking water—A case study. Sci. Total Environ. 470, 469–479.

Borhani, T.N., Saniedanesh, M., Bagheri, M., Lim, J.S., 2016. QSPR prediction of the hydroxyl radical rate constant of water contaminants. Water Res. 98, 344–353.

Calza, P., Massolino, C., Pelizzetti, E., Minero, C., 2008. Solar driven production of toxic halogenated and nitroaromatic compounds in natural seawater. Sci. Total Environ. 398, 196–202.

Chen, B., 2011. Hydrolytic stabilities of halogenated disinfection byproducts: Review and rate constant quantitative structure-property relationship analysis. Environ. Eng. Sci. 28, 385–394.

Cottrell, T. L., 1958. The Strengths of Chemical Bonds, 2nd ed., Butterworth, London.

Criquet, J., Allard, S., Salhi, E., Joll, C.A., Heitz, A., von Gunten, U., 2012. Iodate and iodo-trihalomethane formation during chlorination of iodide-containing waters: Role of bromide. Environ. Sci. Technol. 46, 7350–7357.

Dad, A., Jeong, C.H., Pals, J.A., Wagner, E.D., Plewa, M.J., 2013. Pyruvate remediation of cell stress and genotoxicity induced by haloacetic acid drinking water disinfection by-products. Environ. Mol. Mutagen. 54, 629–637.

Ding, G., Zhang, X., Yang, M., Pan, Y., 2013. Formation of new brominated disinfection byproducts during chlorination of saline sewage effluents. Water Res. 47, 2710–2718.

Echigo, S., Itoh, S., Natsui, T., Araki, T., Ando, R., 2004. Contribution of brominated organic disinfection by-products to the mutagenicity of drinking water. Water Sci. Technol. 50, 321–328.

Gao, Y., Jiang, J., Zhou, Y., Pang, S., Ma, J., Jiang, C., Yang, Y., Huang, Z., Gu, J., Guo, Q., Duan, J., Li, J., 2018. Chlorination of bisphenol S: Kinetics, products, and effect of humic acid. Water Res. 131, 208–217.

Glezer, V., Harris, B., Tal, N., Iosefzon, B., Lev, O., 1999. Hydrolysis of haloacetonitriles: Linear free energy relationship, kinetics and products. Water Res. 33, 1938–1948.

Gong, T., Zhang, X., 2013. Determination of iodide, iodate and organoiodine in waters with a new total organic iodine measurement approach. Water Res. 47, 6660−6669.

Gong, T., Zhang, X., 2015. Detection, identification and formation of new iodinated disinfection byproducts in chlorinated saline wastewater effluents. Water Res. 68, 77–86.

Gong, T., Zhang, X., Liu, W., Lv, Y., Han, J., Choi, K., Li, W., Xian, Q., 2018. Tracing the sources of iodine species in a non-saline wastewater. Chemosphere 205, 643–648.

Du, H., Li, J., Moe, B., McGuigan, C.F., Shen, S., Li, X.-F., 2013. Cytotoxicity and oxidative damage induced by halobenzoquinones to T24 bladder cancer cells. Environ. Sci. Technol. 47, 2823–2830.

Han, J., Zhang, X., 2018. Evaluating the comparative toxicity of DBP mixtures from different

527 disinfection scenarios: A new approach by combining freeze-drying or rotoevaporation with a
528 marine polychaete bioassay. Environ. Sci. Technol. 52, 10552–10561.
529 Han, J., Zhang, X., Liu, J., Zhu X., Gong, T., 2017. Characterization of halogenated DBPs and
530 identification of new DBPs trihalomethanols in chlorine dioxide treated drinking water with
531 multiple extractions. J. Environ. Sci. 58, 83–92.
532 Hua, G., Reckhow, D.A., Abusallout, I., 2015. Correlation between SUVA and DBP formation
533 during chlorination and chloramination of NOM fractions from different sources.
534 Chemosphere 130, 82–89.
535 Jiang, J., Li, W., Zhang, X., Liu, J., Zhu, X., 2018. A new approach to controlling halogenated
536 DBPs by GAC adsorption of aromatic intermediates from chlorine disinfection: Effects of
537 bromide and contact time. Sep. Purif. Technol. 203, 260–267.
538 Jiang, J., Zhang, X., Zhu, X., Li, Y., 2017. Removal of intermediate aromatic halogenated DBPs
539 by activated carbon adsorption: A new approach to controlling halogenated DBPs in
540 chlorinated drinking water. Environ. Sci. Technol. 51, 3435–3444.
541 Jin, X., Peldszus, S., Huck, P.M., 2015. Predicting the reaction rate constants of micropollutants
542 with hydroxyl radicals in water using QSPR modeling. Chemosphere 138, 1–9.
543 Li, W., Zhang, X., Li, X., Lee, J.H.W., 2018. Mystery of the high chlorine consumption in
544 disinfecting a chemically enhanced primary saline sewage. Water Res. 145, 181–189.
545 Li, X.-F., Mitch, W.A., 2018. Drinking water disinfection byproducts (DBPs) and human health
546 effects: Multidisciplinary challenges and opportunities. Environ. Sci. Technol. 52, 1681–
547 1689.
548 Li, Y., Zhang, X., Yang, M., Liu, J., Li, W., Graham, N.J.D., Li, X., Yang, B., 2017. Three-step
549 effluent chlorination increases disinfection efficiency and reduces DBP formation and

toxicity. Chemosphere 168, 1302–1308.

Liu, J., Zhang, X., 2014. Comparative toxicity of new halophenolic DBPs in chlorinated saline wastewater effluents against a marine alga: Halophenolic DBPs are generally more toxic than haloaliphatic ones. Water Res. 65, 64–72.

Liu, J., Zhang, X., Li, Y., 2015. Effect of boiling on halogenated DBPs and their developmental toxicity in real tap water. In Recent Advances in Disinfection By-Products; Karanfil, T., Mitch, W. A., Westerhoff, P., Xie, Y., Eds.; American Chemical Society: Washington, DC, pp 45–60.

Liu, J., Zhang, X., Li, Y., 2017. Photoconversion of chlorinated saline wastewater DBPs in receiving seawater is overall a detoxification process. Environ. Sci. Technol. 51, 58–67.

Lv, X., Zhang, X., Du, Y., Wu, Q., Lu, Y., Hu, H., 2017. Solar light irradiation significantly reduced cytotoxicity and disinfection byproducts in chlorinated reclaimed water. Water Res. 125, 162–169.

Pan, Y., Zhang, X., Wagner, E.D., Osiol, J., Plewa, M.J., 2014. Boiling of simulated tap water: Effect on polar brominated disinfection byproducts, halogen speciation, and cytotoxicity. Environ. Sci. Technol. 48, 149–156.

Qian, Y., Wang, W., Boyd, J.M., Wu, M., Hrudey, S.E., Li, X.-F., 2013. UV-induced transformation of four halobenzoquinones in drinking water. Environ. Sci. Technol. 47, 4426–4433.

Rao, N.N., Dubey, A.K., Mohanty, S., Khare, P., Jain, R., Kaul, S.N., 2003. Photocatalytic degradation of 2-chlorophenol: A study of kinetics, intermediates and biodegradability. J. Hazard. Mater. B101, 301–314.

Richardson, S.D., Plewa, M.J., Wagner, E.D., Schoeny, R., DeMarini, D.M., 2007. Occurrence,

573 genotoxicity, and carcinogenicity of regulated and emerging disinfection by-products in
574 drinking water: A review and roadmap for research. Mutat. Res. 636, 178–242.
575 Richardson, S.D., Postigo, C., 2018. Liquid chromatography–mass spectrometry of emerging
576 disinfection by-products. In: Cappiello, A., Palma, P., (Eds.), Advances in the Use of Liquid
577 Chromatography Mass Spectrometry (LC-MS): Instrumentation Developments and
578 Applications, Elsevier B.V., Amsterdam, Netherlands, pp. 267–295.
579 Roccaro, P., Chang, H., Vagliasindi, F.G.A., Korshin, G.V., 2013. Modeling bromide effects on
580 yields and speciation of dihaloacetonitriles formed in chlorinated drinking water. Water Res.
581 47, 5995–6006.
582 Sankoda, K., Toda, I., Sekiguchi, K., Nomiyama, K., Shinohara, R., 2017. Aqueous secondary
583 formation of brominated, chlorinated, and mixed halogenated pyrene in presence of halide
584 ions. Chemosphere. 171, 399–404.
585 Sharma, V.K., Yang, X., Cizmas, L., McDonald, T.J., Luque, R., Sayes, C.M., Yuan, B.,
586 Dionysiou, D.D., 2017. Impact of metal ions, metal oxides, and nanoparticles on the
587 formation of disinfection byproducts during chlorination. Chem. Eng. J. 317, 777−792.
588 Sharma, V.K., Zboril, R., McDonald, T.J., 2014. Formation and toxicity of brominated
589 disinfection byproducts during chlorination and chloramination of water: A review. J. Eng.
590 Sci. Health Part B, 49, 212−228.
591 Song, H., Addison, J.W., Hu, J., Karanfil, T., 2010. Halonitromethanes formation in wastewater
592 treatment plant effluents. Chemosphere 79, 174–179.
593 Tang, H.L., Chen, Y.C., Regan, J.M., Xie, Y.F., 2012. Disinfection by-product formation
594 potentials in wastewater effluents and their reductions in a wastewater treatment plant. J.
595 Environ. Monitor. 14, 1515–1522.

596 Wang, L., Chen, B., Zhang, T., 2018. Predicting hydrolysis kinetics for multiple types of
597 halogenated disinfection byproducts via QSAR models. Chem. Eng. J. 342, 372–385.
598 Wang, L., Niu, R., Chen, B., Wang, L., Zhang, G., 2017. A comparison of photodegradation
599 kinetics, mechanisms, and products between chlorinated and brominated/iodinated haloacetic
600 acids in water. Chem. Eng. J. 330, 1326–1333.
601 Xiao, R., Ye, T., Wei, Z., Luo, S., Yang, Z., Spinney, R., 2015. Quantitative structure-activity
602 relationship (QSAR) for the oxidation of trace organic contaminants by sulfate radical.
603 Environ. Sci. Technol. 49, 13394–13402.
604 Yan, M., Li, M., Roccaro, P., Korshin, G.V., 2016. Ternary model of the speciation of I/Br/Cl-
605 trihalomethanes formed in chloraminated surface waters. Environ. Sci. Technol. 50, 4468–
606 4475.
607 Yan, M., Roccaro, P., Fabbricino, M., Korshin, G.V., 2018. Comparison of the effects of
608 chloramine and chlorine on the aromaticity of dissolved organic matter and yields of
609 disinfection by-products. Chemosphere 191, 477–484.
610 Yang, Y., Pignatello, J.J., 2017. Participation of the halogens in photochemical reactions in
611 natural and treated waters. Molecules 22, 1684.
612 Yang, M., Liu, J., Zhang, X., Richardson, S.D., 2015. Comparative toxicity of chlorinated saline
613 and freshwater wastewater effluents to marine organisms. Environ. Sci. Technol. 49, 14475–
614 14483.
615 Yang, M., Zhang, X., 2013. Comparative developmental toxicity of new aromatic halogenated
616 DBPs in a chlorinated saline sewage effluent to the marine polychaete *Platynereis dumerilii*.
617 Environ. Sci. Technol. 47, 10868–10876.
618 Yang, M., Zhang, X., 2016. Current trends in the analysis and identification of emerging

disinfection byproducts. Trends Environ. Anal. Chem. 10, 24–34.

Yu, Y., Reckhow, D.A., 2015. Kinetic analysis of haloacetonitrile stability in drinking waters, Environ. Sci. Technol. 49, 11028–10036.

Zhang, D., Chu, W., Yu, Y., Krasner, S.W., Pan, Y., Shi, J., Yin, D., Gao, N., 2018. Occurrence and stability of chlorophenylacetonitriles, a new class of nitrogenous aromatic DBPs, in chlorinated and chloraminated drinking waters. Environ. Sci. Technol. Lett. 5, 394–399.

Zhu, X., Zhang, X., 2016. Modeling the formation of TOCl, TOBr and TOI during chlor (am) ination of drinking water. Water Res. 96, 166–176.

Table 1. Phototransformation of 21 halophenolic DBPs in seawater, observed under 84 h light exposure.

DBP	Phototransformation (%)	k (h^{-1}) [a]	Half-life (h) [a]
2,4,6-trichlorophenol	15.2±1.1	1.96×10^{-3}	353.1
2,4,6-tribromophenol	22.7±2.1	3.07×10^{-3}	226.1
2,4,6-triiodophenol	27.3±2.0	3.80×10^{-3}	182.6
2,6-dichloro-4-nitrophenol	13.6±0.8	1.74×10^{-3}	398.3
2,6-dibromo-4-nitrophenol	15.0±0.5	1.93×10^{-3}	358.3
2,6-diiodo-4-nitrophenol	16.7±0.9	2.18×10^{-3}	318.7
4-chlorophenol	6.3±0.2	7.75×10^{-4}	894.8
4-bromophenol	8.0±0.4	9.93×10^{-4}	698.3
4-iodophenol	9.8±0.6	1.23×10^{-3}	564.5
3,5-dichloro-4-hydroxybenzaldehyde	29.4±1.1	4.14×10^{-3}	167.2
3,5-dibromo-4-hydroxybenzaldehyde	35.0±1.6	5.13×10^{-3}	135.2
3,5-diiodo-4-hydroxybenzaldehyde	76.7±4.2	1.73×10^{-2}	40.0
2,4-dichlorophenol	37.7±1.4	5.63×10^{-3}	123.0
2,6-dichlorophenol	12.2±2.0	1.55×10^{-3}	447.5
2,4-dibromophenol	49.5±2.8	8.13×10^{-3}	85.2
2,6-dibromophenol	29.4±1.6	4.14×10^{-3}	167.2
2-bromo-4-chlorophenol	47.7±2.8	7.72×10^{-3}	89.8
4-bromo-2-chlorophenol	35.8±2.1	5.28×10^{-3}	131.4
5-chlorosalicylic acid	88.8±4.8	2.61×10^{-2}	26.6
5-bromosalicylic acid	98.7±2.5	1.21×10^{-1} [b]	5.7 [b]
2,5-dibromohydroquione	100	4.62×10^{-1} [c]	1.5 [c]

[a] The results were calculated per the pseudo-first-order phototransformation.
[b] The results were obtained in our previous study (Liu et al., 2017).
[c] The concentration of 2,5-dibromohydroquinone was undetectable by the light exposure time of 84 h. Per our previous study (Liu et al., 2017), 2,5-dibromohydroquinone completely transformed within 3 h light exposure.

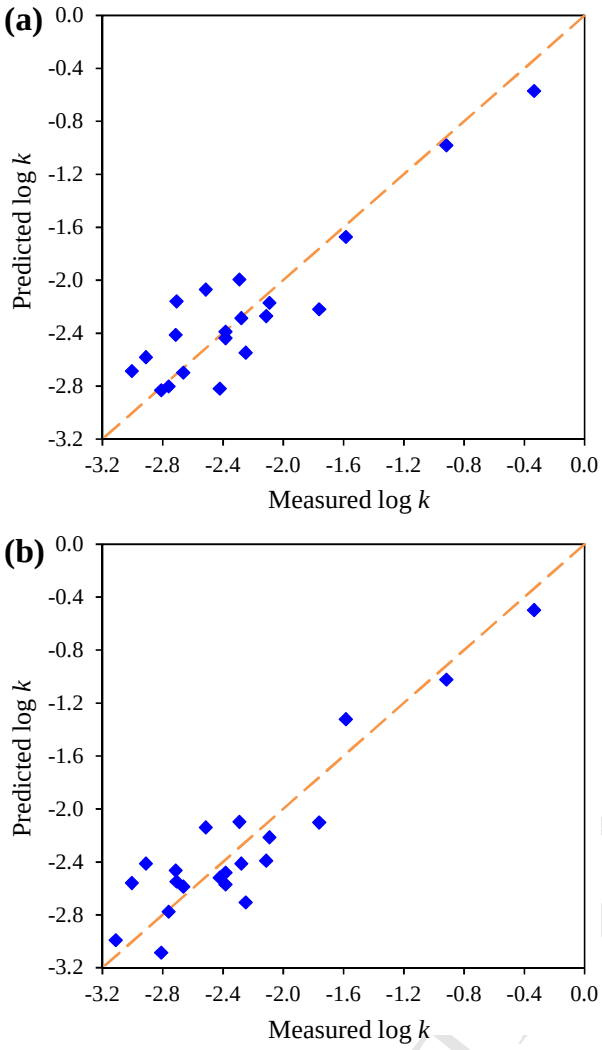

Fig. 1. (a,b) Plots of measured log *k* of the 21 halophenolic DBPs against log *k* values predicted from Equations (3) and (5), respectively.

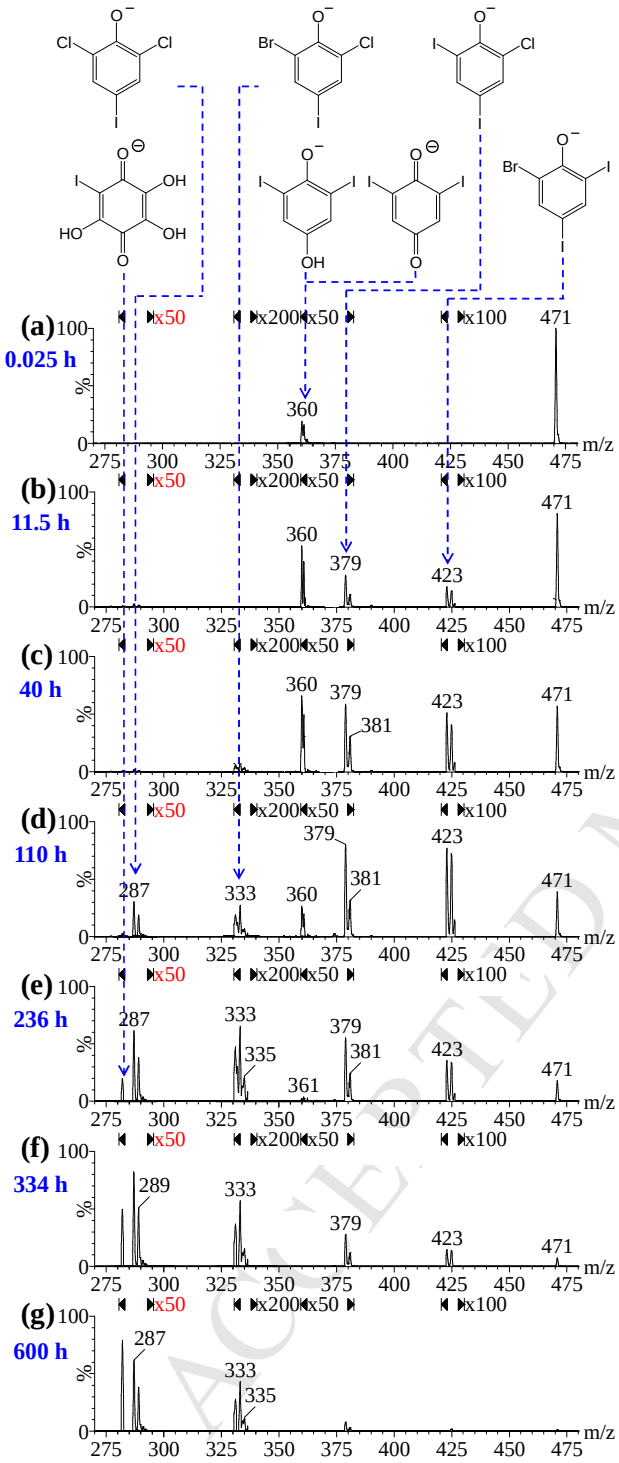

Fig. 2. ESI-tqMS PIS spectra of *m/z* 126.9 of 2,4,6-triiodophenol seawater solutions with the light exposure times of (a) 0.025, (b) 11.5, (c) 40, (d) 110, (e) 236, (f) 334, and (g) 600 h. The y-axes are all on the same scale. Proposed structures of some ions and ion clusters are shown at the top of the figure. For chlorodiiodophenol, bromodiiodophenol and dichloroiodophenol, isomers were detected using UPLC/ESI-tqMS MRM scans.

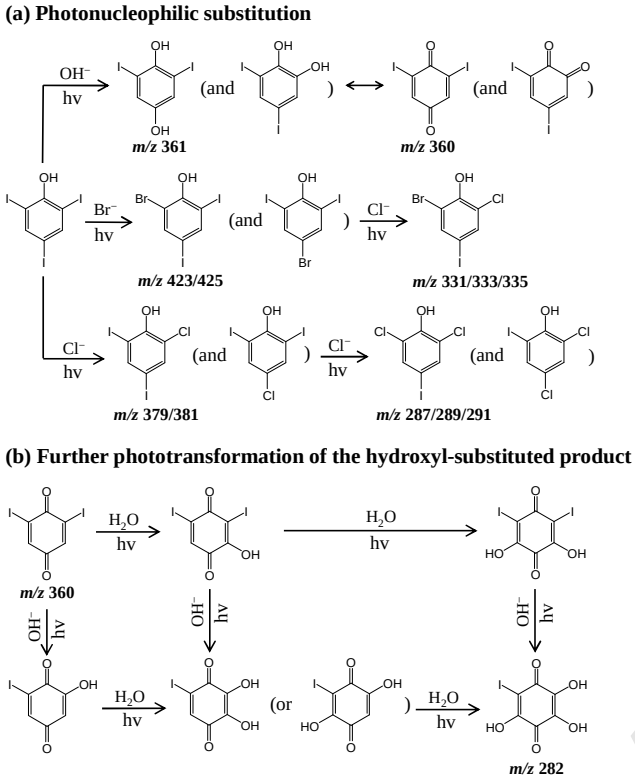

Fig. 3. Phototransformation pathway of 2,4,6-triiodophenol in seawater: **(a)** photonucleophilic substitution of 2,4,6-triiodophenol, and **(b)** further phototransformation of the hydroxyl-substituted product. The products were tentatively proposed. The structures marked with *m/z* values indicate that the corresponding molecular ions or ions clusters were detected by ESI-tqMS PIS of *m/z* 126.9.

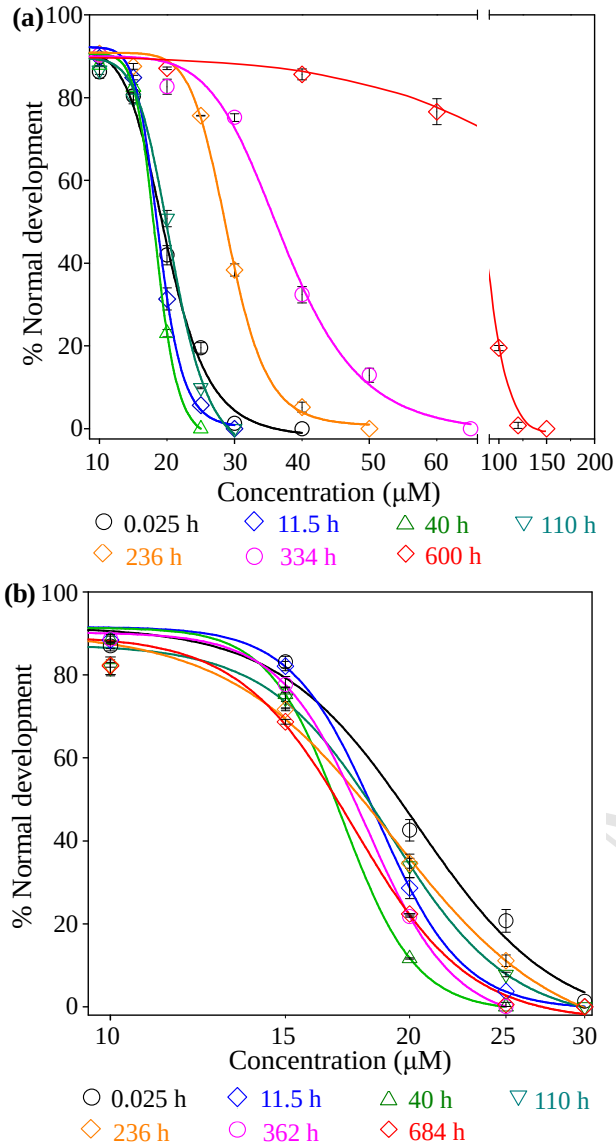

Fig. 4. Normal development percentages of the marine polychaete *P. dumerilii* in the **(a)** "2,4,6-triiodophenol" and **(b)** "2,6-diiodo-4-nitrophenol" solutions with different light exposure times. The x-axes indicate the concentrations of 2,4,6-triiodophenol and 2,6-diiodo-4-nitrophenol in the concentrated test sample prior to phototransformation.

Highlights

- Photolysis rates of halophenolic DBP analogues followed iodo- > bromo- > chloro-.
- A QSAR model was developed for the photolysis of halophenolic DBPs.
- Iodophenolic DBPs phototransformed to the bromo-, chloro- and hydroxy-counterparts.
- The hydroxy-counterparts (halo(hydro)quinone) were more toxic than the parent DBPs.
- Further phototransformation of halo(hydro)quinone was a detoxification process.